

Limited Imitation Contagion on Random Networks: Chaos, Universality, and Unpredictability

Peter Sheridan Dodds,^{1,*} Kameron Decker Harris,^{1,†} and Christopher M. Danforth^{1,‡}

¹*Department of Mathematics & Statistics, Vermont Complex Systems Center,
& the Vermont Advanced Computing Core, The University of Vermont, Burlington, VT 05401.*

(Dated: August 2, 2012)

We study a family of binary state, socially-inspired contagion models which incorporate imitation limited by an aversion to complete conformity. We uncover rich behavior in our models whether operating with probabilistic or deterministic individual response functions, both on dynamic or fixed random networks. In particular, we find significant variation in the limiting behavior of a population's infected fraction, ranging from steady-state to chaotic. We show that period doubling arises as we increase the average node degree, and that the universality class of this well known route to chaos depends on the interaction structure of random networks rather than the microscopic behavior of individual nodes. We find that increasing the fixedness of the system tends to stabilize the infected fraction, yet disjoint, multiple equilibria are possible depending solely on the choice of the initially infected node.

PACS numbers: 89.65.-s, 87.19.Xx, 87.23.Ge, 05.45.-a

The structure and dynamics of real, complex networks remains an open area of great research interest, particularly in the realm of evolutionary processes acting on and within networked systems [1–6]. Here, motivated by considerations of social contagion—the spreading of ideas and behaviors between people through social networks and media—we explore an idealized, binary-state social contagion model in which individuals choose to be like others but only up to a point: they do not want to be like everyone else [7–10]. We term such behavior ‘Limited Imitation Contagion.’ We build naturally on previous studies of threshold models of contagion [11–14], and our model can also be seen as a specific subfamily of dynamical Boolean network models [15, 16]. We show how macroscopic network structure overrides microscopic details, and we find complex dynamics whose character moves from universal and predictable to particular and unpredictable as we allow the system to become increasingly deterministic.

In constructing our model, our main interest is in understanding how spreading by Limited Imitation Contagion on random networks behaves under three main tunable conditions: (1) Social awareness: the rate of contact between individuals; (2) Social variability: the extent to which friendships are fixed; and (3) Social influence: the character of individuals’ responses to the behavior of others.

To begin with, we consider a binary state model [17] for which individuals are either in a base state S_0 or an alternate state S_1 . We assume individuals interact over an uncorrelated random network (we treat correlated networks in [18]), which may be dynamic or fixed. For simplicity, and due to the richness of the dynamics we find, we employ standard Erdős-Rényi networks which possess Poisson degree distributions. We take time to be discrete ($t = 0, 1, 2, \dots$), and we prescribe each node’s degree k

at $t = 0$. In a dynamic network, when node i updates, it samples the states of k_i randomly chosen nodes (i.e., the system is a random mixing model with non-uniform contact rates). For a fixed network, node i repeatedly samples the same k_i nodes. We further restrict our attention to single-seed contagion processes wherein all nodes are in state S_0 at time $t = 0$, with one randomly chosen node in state S_1 .

The contagion process is manifested through the response functions of individual nodes. We allow nodes to update synchronously (in [18], we consider a fourth condition of social synchrony—the degree of timing coherence between individual decisions). Node i ’s response function $F_i : [0, 1] \mapsto [0, 1]$ gives the probability that node i will be in state S_1 upon updating, where the argument taken by F_i is the fraction of nodes sampled by node i that are currently in state S_1 , $\phi_{i,t}$. We investigate two kinds of response functions, probabilistic and deterministic, both of which incorporate the characteristic of the adoption probability growing with low and then diminishing with high values of perceived popularity.

In Fig. 1A, we show an example of a probabilistic response function, the tent map, which is defined as $T_r(x) = rx$ for $0 \leq x \leq \frac{1}{2}$ and $r(1 - x)$ for $\frac{1}{2} \leq x \leq 1$. Taking the $r = 2$ case—for which the iterative map of the interval is fully chaotic and the invariant density χ is uniform on $[0, 1]$ —node i adopts state S_1 with probability $T_2(\phi_{i,t})$. We use the tent map T_2 for several reasons: (1) As a standard iterative map of the interval, the tent map’s dynamics are both interesting and well understood [19]; (2) The tent map captures a probabilistic flavor of the adopt-when-novel, drop-when-ubiquitous behavior we aim to model; and (3) We can construct a simple and elegant connection with deterministic contagion processes which we describe next.

In Fig. 1B, we show an example of a deterministic

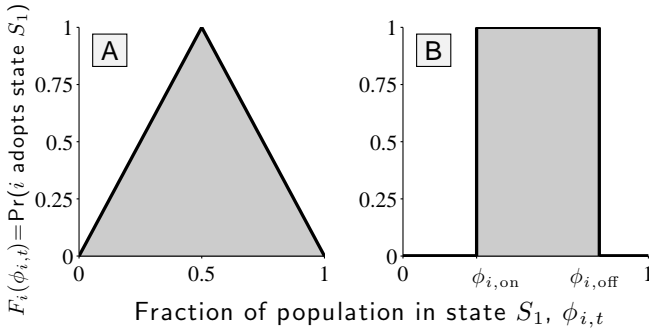


FIG. 1: Examples of probabilistic and deterministic response functions capturing Limited Imitation Contagion dynamics. At each time t , nodes use their given response functions to update their own state based on the perceived fraction of their neighbors in state S_1 , $\phi_{i,t}$. We construct the tent map T_2 (see main text) shown in (A) by averaging over deterministic response functions of the kind shown in (B) by considering a family of the latter with ‘on’ and ‘off’ thresholds uniformly distributed in $[0, \frac{1}{2}]$ and $[\frac{1}{2}, 1]$ respectively. We then build networked systems whose macroscopic character is tent map-like but differ strongly at the microscopic level.

response function which is characterized by ‘on’ and ‘off’ thresholds, ϕ_{on} and ϕ_{off} . Node i will only adopt or remain in state S_1 if it perceives the fraction of others in state S_1 to lie between its on and off thresholds: $\phi_{i,\text{on}} \leq \phi_{i,t} < \phi_{i,\text{off}}$.

Now, for these deterministic ‘on-off’ response functions, we examine the special case where ϕ_{on} is distributed uniformly on $[0, \frac{1}{2}]$ and ϕ_{off} likewise on $[\frac{1}{2}, 1]$. Averaging over all deterministic response functions created in this way, we obtain precisely the tent map T_2 . Collectively, we then have the same on-average behavior in both the probabilistic and deterministic cases, and this allows us to profitably explore the effect of varying the specific response dynamics at the micro level as well as interaction patterns.

We now examine the behavior of four subfamilies of our model that vary in terms of node response functions being probabilistic or deterministic (P or D), and whether or not network connections randomly rewire or are fixed (R or F). We refer to these model classes as P-R, P-F, D-R, and D-F. Each class is indexed by the parameter of average node degree k_{avg} , and, as per our design, all four systems have the same on-average response functions (the tent map T_2) and degree distribution (Poisson).

Our first focus is on the long term behavior of these four networked systems. Key to our understanding are the well-known behaviors of the tent and logistic maps acting iteratively on the unit interval, the former given above and the latter by $L_r(x) = rx(1-x)$. We reproduce the orbit diagrams for these models in Figs. 2A and B. Both systems are controlled by amplitude parameter r , whose increase leads to changes in their invariant densities, famously resulting in the bifurcation diagram for

the logistic map. The two maps, while topologically conjugate, produce distinct bifurcation diagrams.

As we show in Fig. 2C–F, the signature of the microscopic response function of the tent map is erased by the network dynamics of the four model classes. Macroscopically, we see four orbit diagrams analogous to the logistic map’s characteristic bifurcation diagram, corresponding to Fig. 2B rather than Fig. 2A. We see that increasing the average connectivity of the network k_{avg} is equivalent to increasing the logistic map’s amplitude parameter r , and the system moves along the period-doubling route to chaos.

While appearing to belong to the same universality class, the orbit diagrams of the four models differ importantly in detail, most profoundly for the fully deterministic D-F class. First, we observe the four systems produce three distinguishable orbit diagrams, since for large enough systems, the two random mixing classes P-R and D-R must exhibit the same macroscopic behavior. For the D-R class, random rewiring overwhelms the fact of each node having a fixed deterministic response function.

We are able to comprehensively explore the P-R and D-R models via both simulation and analysis, finding excellent agreement. We show only simulation results here, making full comparisons in [18], and record the core analytic description below by directly following the P-R model. The infected fraction ϕ_t (equivalently, the probability that a random node is infected at time t) is given by $\phi_{t+1} = \sum_{k=0}^{\infty} P_k G_k(\rho_t)$, where P_k is the probability a node samples the states of k randomly chosen nodes; G_k is the probability that such a node is active at time step t ; and ρ_t is the probability that a randomly chosen edge emanates from a node infected at time t . The dynamics are encoded in the update map for the edge infection probability:

$$\rho_{t+1} = \sum_{k=0}^{\infty} \frac{k P_k}{k_{\text{avg}}} G_k(\rho_t), \quad (1)$$

where $G_k(\rho_t) = \sum_{j=0}^k \binom{k}{j} \rho_t^j (1 - \rho_t)^{k-j} f(j/k)$, and where $f(x)$ is the node response function (here, the tent map). In [18], we show that in the limit of infinite average degree k_{avg} and providing the width of the degree distribution grows sublinearly with respect to k_{avg} , the dynamics approach that of the response function f . However, in the approach to that limit, the form of the $\{G_k\}$ induces a quadratic maximum for the edge infection update map, Eq. (1), and the system thereby shares the universality class of the logistic map. Thus, in terms of the emergent, global behavior, we see that the interaction pattern of the network overrides and masks the microscopic response function. More generally, we find the same universal behavior for any unimodal, concave response function [18].

Moving to the fixed network models P-F and D-F, we find that these are less amenable to direct analysis, and

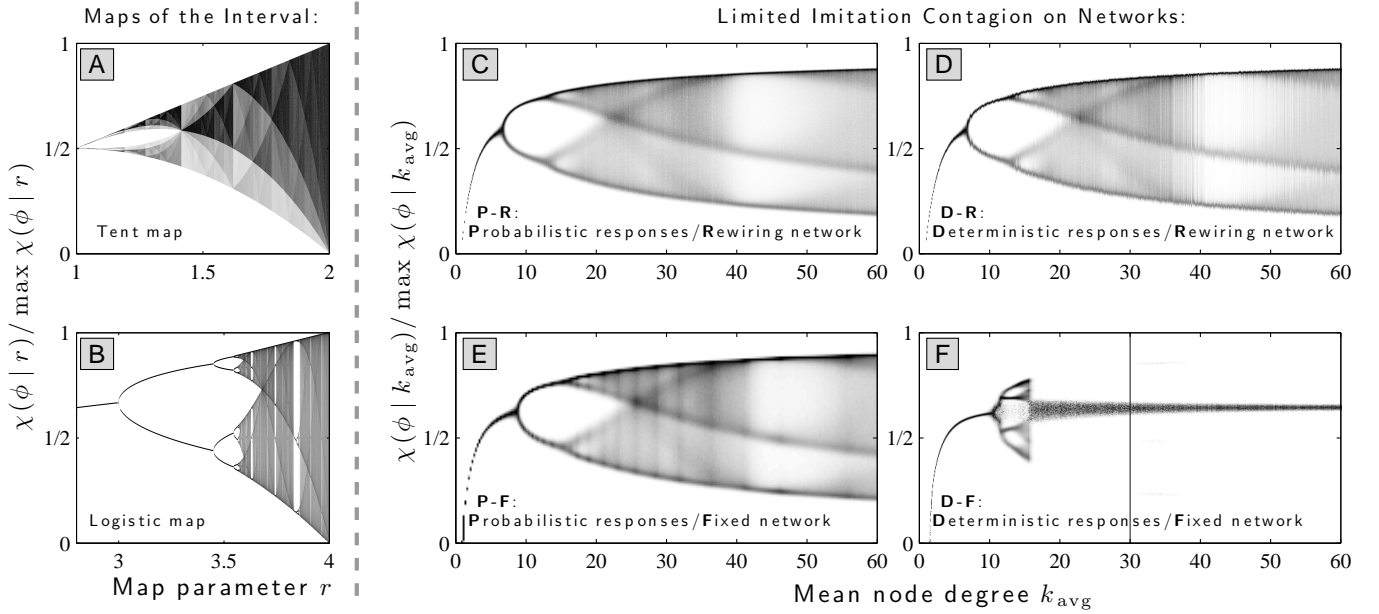


FIG. 2: Comparison of bifurcation diagrams for networked systems with Limited Imitation Contagion based on tent-map response functions. (A) and (B): For reference, standard bifurcation diagrams for the tent map and the logistic map operating as maps of the unit interval, showing distinct universality classes. The vertical axis is normalized invariant density χ . (C–F): Orbit diagrams for Limited Imitation Contagion acting on standard random networks for four model classes with probabilistic or deterministic responses and network interactions as indicated. The tunable parameter is average degree k_{avg} . In F, the vertical line indicates $k_{\text{avg}} = 30$, the system examined in Fig. 3. Simulation details: network size $N=10^4$; one random seed per network; granularity of 0.1 in k_{avg} ; binning size of 0.001 in ϕ ; for P-R, D-R, and P-F systems, we ran simulations for 10^4 time steps on 10^3 networks, ignoring the first 10^3 values of ϕ_t ; and for D-F systems, which exhibit long transient behavior (see text), we ran simulations for 10^5 time steps on 200 networks, ignoring the first 5×10^4 time steps.

report our findings for simulation results only. Considering the P-F model first, we see in Fig. 2E that the orbit diagram has slightly moved to the right—the bifurcation points now occur for slightly higher values of k_{avg} . Thus, the fixedness of the network appears to induce some modest changes in the dynamics, though we cannot discount finite size effects.

Our final model class, D-F—to whose description we devote the remainder of the paper—is the most structured, and it generates considerably distinct and intricate behavior. Once the network and set of response functions is realized, the system is now completely deterministic, and we find surprising changes in the system’s behavior at both macroscopic and microscopic scales. In Fig. 2F, we see that the orbit diagram for the D-F model collapses abruptly after several rounds of period doubling, which are themselves relatively compressed. Our simulations suggest that above an average degree of $k_{\text{avg}} \simeq 16$, the macroscopic dynamics always collapse. The collapse appears to favor a fixed point macroscopic state, around $\phi = 2/3$, which is the fixed point of the tent map T_2 . However, a closer examination of the D-F class’s potential dynamics reveals a far more subtle story.

In Fig. 3, we summarize the possible dynamics of a lone realized network ($N=10^4$, $k_{\text{avg}}=30$) with a single set of

fixed deterministic response functions (we explore other values of k_{avg} in [18]). We exhaustively ran $N = 10^4$ tests of the system’s behavior by separately seeding each individual node. Of these, 7865 contagion events were successful leading to long term non-zero infection levels. Figs. 3A–C show three example system evolutions for the same network, differing only by seed node. In each case, the early dynamics of ϕ have a chaotic appearance with a broad period three pattern, but then all collapse sharply to (apparently, see below) different kinds of period 2 behavior.

The time to collapse t_c varies greatly, with Fig. 3C showing an example requiring over 30,000 time steps and over 3×10^8 individual node updates. In Fig. 3D, we provide the complementary cumulative distribution for collapse times. The semi-log scale indicates that an exponential decay for $t_c < 20,000$ covers the majority of cases. A set of exceptional dynamics last for much longer, with one group ending at around $t_c \simeq 30,000$, and another isolated set distributed around $t_c \simeq 25,000$. Even after the dynamics collapse, we see that on the order of 10% of all nodes change state in each time step. We find similar behavior in for other values of k_{avg} and for larger systems of size $N = 10^5$.

We turn lastly to the behavior after the collapse. We

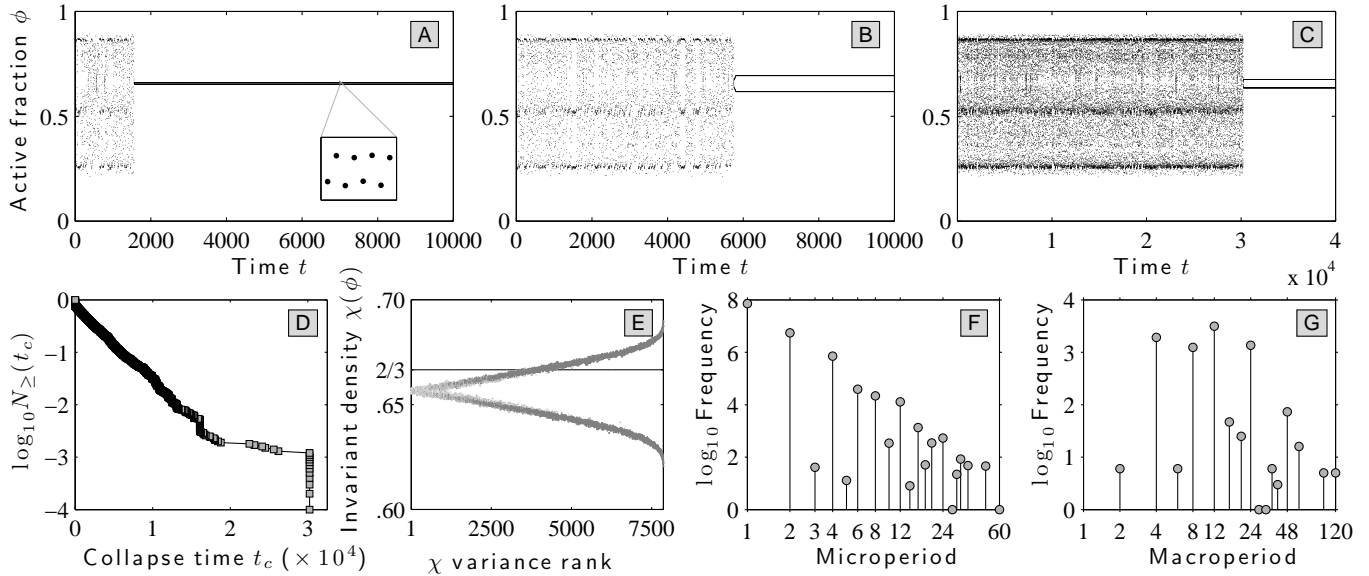


FIG. 3: Comprehensive survey of the possible Limited Imitation Contagion dynamics for a single fixed random network ($k_{\text{avg}}=30$) with its $N=10^4$ nodes having fixed deterministic response functions. We ran N simulations, activating each node as a single seed and allowed the fully deterministic dynamics to run until collapse. (A-C): Examples of dynamics for three systems showing widely varying collapse time t_c and different post-collapse dynamics. The inset in A shows one cycle of the underlying period 8 behavior; the post-collapse dynamics in B and C have periods 24 and 8. (D): Complementary cumulative distribution of collapse times. (E): Invariant densities; (F): Histogram of post-collapse microperiods; (G): Histogram of post-collapse macroperiods.

call the period of ϕ the system’s ‘macroperiod’, and the periods of individual nodes ‘microperiods’. Fig. 3E shows the invariant density χ for all seeds post collapse, ordered by χ ’s variance (contagion events that fail are not included). The gray scale indicates frequency of the invariant density, and the blurring shows that higher order periods underlie the apparent macroperiod 2 behavior. For example, the macroperiods of the time series in Figs. 3A–C are 8, 24, and 8. We also note that the tent map’s fixed point of $2/3$ (horizontal line in Fig. 3E) is not the center of the invariant densities, and that this is perhaps a finite size effect.

In Fig. 3F and G, we provide complete histograms of all post-collapse microperiods and macroperiods (again ignoring failed spreading events). We see that microperiods such as 1, 2, 4, 12, 24, and 48 form a dominant envelope, and while there are occasional instances of microperiods 3 and 5, many odd-numbered microperiods are absent. We find that the most common resultant macroperiods are 4, 8, 12, and 24; that a pure macroperiod 2 is relatively rare ($< 0.1\%$), and that the largest observed macroperiod is 120 (5 instances). Again, all of these outcomes are deterministic, depending only on the choice of initial seed.

To conclude, in abstracting from a real world problem, we have constructed a rich networked-based model of Limited Imitation Contagion that allows us to deeply explore the effects of increasing fixedness in a well-defined

fashion. Some next steps would include, via simulation and analysis, exploring the long term behavior for the D-F class when there is no collapse [18], investigating how collapse time distributions scale with N for the D-F class; similarly testing other contagion mechanisms across systems of increasingly fixed microscopic structure; and examining these Limited Imitation Contagion models on real networks and classes of naturally occurring ones such as scale-free networks [20].

The authors thank A. Mandel and D. J. Watts for encouragement, and are grateful for the computational resources provided by the Vermont Advanced Computing Core supported by NASA (NNX 08A096G). KDH was supported by VT-NASA EPSCoR; CMD was supported by NSF grant DMS-0940271; PSD was supported by NSF CAREER Award #0846668.

* Electronic address: peter.dodds@uvm.edu

† Electronic address: kameron.harris@uvm.edu

‡ Electronic address: chris.danforth@uvm.edu

[1] M. E. J. Newman, SIAM Review **45**, 167 (2003).

[2] D. J. Watts and P. S. Dodds, Journal of Consumer Research **34**, 441 (2007).

[3] V. Colizza, A. Barrat, M. Barthelmey, A.-J. Valleron, and A. Vespignani, PLoS Medicine **4**, e13 (2011).

[4] S. Wuchty, B. F. Jones, and B. Uzzi, Science **316**, 1036 (2007).

- [5] Y.-Y. Liu, J.-J. Slotine, and A.-L. Barabási, *Nature* **473**, 167 (2011).
- [6] C. A. Hidalgo, B. Klinger, A.-L. Barabási, and R. Hausman, *Science* **317**, 482 (2007).
- [7] M. S. Granovetter and R. Soong, *Journal of Economic Behavior & Organization* (1986).
- [8] J. Ugander, L. Backstrom, C. Marlow, and J. Kleinberg, *Proc. Natl. Acad. Sci.* **109**, 5962 (2012).
- [9] G. Simmel, *Am. J. Sociol.* **62**, 541 (1957).
- [10] Our model is distinct from traditional coupled maps [21], having binary rather than continuous node states, and exhibits fundamentally different behavior.
- [11] T. C. Schelling, *J. Math. Sociol.* **1**, 143 (1971).
- [12] M. Granovetter, *Am. J. Sociol.* **83**, 1420 (1978).
- [13] D. J. Watts, *Proc. Natl. Acad. Sci.* **99**, 5766 (2002).
- [14] J. P. Gleeson, *Phys. Rev. E* **77**, 046117 (2008).
- [15] S. A. Kauffman, *J. Theor. Biol.* **22**, 437 (1969).
- [16] M. Aldana, S. Coppersmith, and L. P. Kadanoff, in *Perspectives and Problems in Nonlinear Science*, edited by E. Kaplan, J. E. Marsden, and K. R. Sreenivasan (Springer, New York, 2003), chap. 2, pp. 23–90.
- [17] T. C. Schelling, *J. Conflict Resolut.* **17**, 381 (1973).
- [18] K. D. Harris, C. M. Danforth, and P. S. Dodds (2012), in preparation.
- [19] K. T. Alligood, T. D. Sauer, and J. A. Yorke, *Chaos: An Introduction to Dynamical Systems* (Springer, 1996).
- [20] A.-L. Barabási and R. Albert, *Science* **286**, 509 (1999).
- [21] K. Kaneko, *Prog. Theor. Phys.* **72**, 480 (1984).